Magnetic Resonance Imaging 61 (2019) 9–15

Contents lists available at ScienceDirect

Magnetic Resonance Imaging

journal homepage: www.elsevier.com/locate/mri

Original contribution

# Using amide proton transfer to identify cervical squamous carcinoma/adenocarcinoma and evaluate its differentiation grade

Nan Meng[a,1], Jing Wang[a,1], Jing Sun[b,1], Wenling Liu[a], Xuejia Wang[a], Minghuan Yan[a], Akshay Dwivedi[a], Dandan Zheng[c], Kaiyu Wang[c], Dongming Han[a,*]

[a] Department of MR, the First Affiliated Hospital, Xinxiang Medical University, 88 Jiankang Road, Weihui 453100, PR China
[b] Department of Pediatrics, Zhengzhou Central Hospital, Zhengzhou University, 195 Tongbai Road, Zhengzhou 450000, PR China
[c] MR Research China, GE Healthcare, Beijing 100000, PR China

ARTICLE INFO

*Keywords:*
Cervical squamous carcinoma (CSC)
Cervical adenocarcinoma (CA)
Amide proton transfer-weighted imaging (APTWI)

ABSTRACT

*Purpose:* To explore the possibility of using amide proton transfer-weighted imaging (APTWI) for the identification and diagnosis of cervical squamous carcinoma (CSC), cervical adenocarcinoma (CA) and different levels of CSC.

*Materials and methods:* Seventy-six patients with newly diagnosed uterine cervical cancer (UCC) were studied prior to treatment, including 20 with poorly differentiated (Grade 3) CSC, 23 with moderately differentiated (Grade 2) CSC, 17 with well-differentiated (Grade 1) CSC, and 16 with CA (13 with poorly differentiated (Grade 3) CA and 3 with moderately differentiated (Grade 2) CA). Differences in the magnetization transfer ratio at 3.5 ppm (MTRasym (3.5 ppm)) were identified between CSC and CA and between high-level (Grade 3) CSC and low-level (Grade 2 and Grade 1) CSC, as well as among all three grades of CSC differentiation. Receiver operating characteristic (ROC) curve analysis was used to evaluate the diagnostic thresholds and performance of the parameters. Spearman correlation analysis was used to examine the correlation between the MTRasym (3.5 ppm) and histological grade.

*Results:* The MTRasym (3.5 ppm) in CA was higher than that in CSC (P = 0.001). The MTRasym (3.5 ppm) in high-level CSC was higher than that in low-level CSC (P = 0.001). The MTRasym (3.5 ppm) was positively correlated with the grade of CSC differentiation (r = 0.498, P = 0.001). The MTRasym (3.5 ppm) in Grade 3 CSC was higher than that in Grade 2 and Grade 1 CSC (P = 0.02/0.01). No significant difference in the MTRasym (3.5 ppm) was found between Grade 2 CSC and Grade 1 CSC (P = 0.173). The area under the ROC curve (AUC) for the MTRasym (3.5 ppm) in distinguishing CSC and CA was 0.779, with a cut-off, sensitivity, and specificity of 2.97%, 60.0% and 82.5%, respectively. The AUC for distinguishing high-/low-level CSC was 0.756, with a cut-off, sensitivity, and specificity of 3.29%, 68.8% and 83.3%, respectively.

*Conclusion:* APTWI may be a useful technique for the identification and diagnosis of CSC, CA and different levels of CSC, which may have an important impact on clinical strategies for treating patients with UCC.

## 1. Introduction

Uterus cervical cancer (UCC) is the third most common malignant tumor in the female reproductive system and has the highest mortality rate [1,2]. Its incidence is increasing year by year in developing countries, and a younger trend is evident [3]. The prognosis of UCC is closely related to the pathology type and the grade of differentiation. Cervical adenocarcinoma (CA) can easily invade the cervical interstitium and vascular and lymph spaces and is associated with a poor prognosis [4]. Studies have shown that the 5-year survival rate of CA is approximately 10%–20% lower than that of cervical squamous carcinoma (CSC) [5]. CSC accounts for approximately 75%–80% of the total incidence of UCC. Poorly differentiated CSC has specific biological behavior and can easily engender local infiltration and distant metastasis, seriously affecting the prognosis of patients [6,7]. Traditional multiple punch biopsy under vaginoscopy is easily affected by factors such as lesion size, sampling accuracy, and operator experience [8], leading to certain differences between the results and final pathology. In addition, CA is found mostly in the cervical canal, complicating sampling and leading to low screening accuracy. Studies have shown that the

* Corresponding author.
*E-mail addresses:* Kaiyu.Wang1@ge.com (K. Wang), mnhcgz@126.com (D. Han).
[1] These authors contributed equally to this work and should be considered co-first authors.

https://doi.org/10.1016/j.mri.2019.05.005
Received 31 January 2019; Received in revised form 28 April 2019; Accepted 4 May 2019

cytological examination of approximately 24.3% of patients with invasive CA shows negative results [9]. Therefore, accurately evaluating the pathology type and the grade of differentiation of UCC is beneficial to the prognosis of patients.

Currently, magnetic resonance imaging (MRI) is the dominant imaging modality for diagnosing, staging and evaluating the treatment response in UCC. However, conventional imaging methods can only reflect the morphological features of a lesion and cannot evaluate the pathology type and grade of differentiation. Recent studies have shown differences in protein and peptide contents in tumor tissues with different pathology types and grades of differentiation [10–12]. Traditional protein detection methods, such as protein electrophoresis analysis of ex vivo tissue and enzyme activity detection, have poor real-time performance, and the sampling procedure may cause damage to the human body. Magnetic resonance spectroscopy (MRS) can be used for non-invasive measurement of the content of macromolecular substances in tissues, but its application is restricted by its disadvantages such as a long scan time and poor quantitative accuracy. Amide proton transfer-weighted imaging (APTWI) is a chemical exchange saturation transfer (CEST) imaging technology [13] and an MRI technology used to detect mobile protein and peptide contents in living tissue without using an exogenous magnetic resonance contrast agent [14]. The imaging principle involves the use of a radiofrequency saturation pulse at a specific frequency offset of 3.5 ppm downfield from the water resonance signal to saturate the amide protons on mobile proteins/peptides in cells. Due to the chemical exchange between the amide protons and the hydrogen protons of water, the hydrogen protons of some of the water will be saturated, and after repeated chemical exchanges, the water signal is reduced. Therefore, the concentration or exchange rate of the amide protons can be indirectly determined from the degree of water signal reduction [13,15,16].

APTWI has been proven to be useful for the diagnosis and classification of brain tumors [17–20] and neck tumors [21], identification and evaluation of benign and malignant lesions of the prostate [22], and evaluation of the grade of malignancy of rectal tumors [23]. This research aims to explore the possibility of using APTWI for the identification and diagnosis of CSC, CA and different levels of CSC and is expected to provide a reference for relevant clinical diagnosis and treatment methods.

## 2. Materials and methods

### 2.1. Patients

This research was approved by the Ethics Committee of our hospital, and all patients signed an informed consent form before being scanned. Between June 2017 and August 2018, 110 consecutive female patients with cervical lesions underwent MRI (Fig. 1). Of these patients, 34 subjects were excluded for the following reasons: (1) the presence of noncervical cancer (n = 8); (2) unavailable histopathological grades because operations were not performed (n = 7); (3) previous chemoradiotherapy before the examination (n = 7); and (4) an incomplete scanning sequence or the presence of obvious motion/metal/air imaging artifacts (n = 12). The final study population consisted of 76 patients (mean age, 62 years; age range, 46–77 years) with newly diagnosed UCC.

These patients were assessed based on histological features as follows: well-differentiated, moderately differentiated and poorly differentiated disease, which were marked as Grade 1 (G1), Grade 2 (G2) and Grade 3 (G3), respectively. The G1 group and G2 group were classified as the low-level group, and the G3 group was classified as the high-level group.

### 2.2. MRI technique

A pelvic MRI scan was performed using a 3.0-T MR scanner (Discovery MR750, GE Healthcare, Milwaukee, Wisconsin), and a 32-channel phased-array torso coil was used for imaging the pelvis. Scanning ranged from up to the anterior superior iliac spine down to the symphysis pubis. Before the examination, patients were required to have a bladder full of urine, and a gel sponge was applied for vaginal packing to ensure that the uterus was in a moderately forward state for observation and scanning of the lesion. Sagittal T2-weighted imaging (T2WI) without fat suppression was performed using the following parameters: field of view (FOV), 36 × 28 $cm^2$; slice thickness, 6.0 mm; spacing, 2.0 mm; number of slices, 20; repetition time (TR), 6000 ms; echo time (TE), 81 ms; and matrix, 320 × 224. Axial fat-suppressed T2WI and T1-weighted imaging (T1WI) were performed using the following parameters: FOV, 36 × 36 $cm^2$; slice thickness, 5.0 mm; spacing,

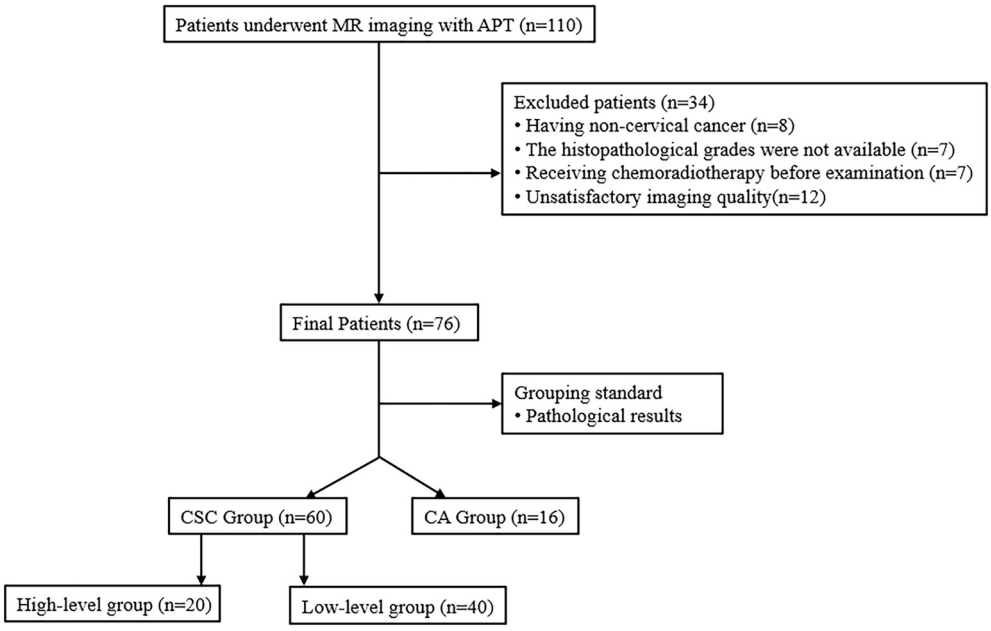


**Fig. 1.** Flow diagram of the patient selection process.

1.0 mm; number of slices, 20; TR, 5455/605 ms, TE, 109/8 ms, and matrix, 320 × 224. Axial diffusion-weighted imaging (DWI) was performed using the following parameters: FOV, 36 × 36 $cm^2$; slice thickness, 5.0 mm; spacing, 1 mm; b-value [24], 1000 s/$mm^2$; number of excitations (NEX), 6; TR, 6000 ms; TE, 59 ms; and matrix, 128 × 128.

The patients did not undergo any form of enhanced examination for 24 h prior to APTWI to avoid interference with the APTWI signal [25]. After the DWI scan was completed, under the guidance of an experienced radiologist, all layers containing the tumor subject were scanned using the APTWI sequence layer by layer. The sequence used here is Chemical exchange saturation transfer (CEST) with EPI acquisition, and the scanning parameters are as follows: TR, 3000 ms; echo time (TE), 12.0 ms; FOV, 36 × 36 $cm^2$; matrix, 128 × 128; layer thickness, 5 mm; saturation pulse (RF), 2.0 μT; saturation time, 500 ms (4 pulses were applied for saturation). We used 52 frequencies for these sequences, with 1 NEX resulting in 52 images. Frequency list: 5000, 5000, 5000, ± 600, ± 575, ± 550, ± 525, ± 500, ± 475, ± 450, ± 425, ± 400, ± 375, ± 350, ± 325, ± 300, ± 275, ± 250, ± 225, ± 200, ± 175, ± 150, ± 125, ± 100, ± 75, ± 50, ± 25 Hz, the scaning time, 2 min 36 s. The MTRasym (3.5 ppm) was calculated at 3.5 ppm, and $B_0$ correction was performed by shifting the minimum signal of the z spectrum to 0 Hz.

### 2.3. Image analysis

All data were analyzed and processed on a workstation (Advantage workstation 4.6, GE Healthcare, Milwaukee, Wisconsin) and post-processed using the APTWI processing toolbox available within Functool software. The data were measured independently by two experienced radiologists. First, the radiologists measured the tumor volume: tumor volume = tumor area at each level × (layer thickness + layer spacing). Then, they measured the tumor MTRasym (3.5 ppm) by carefully reviewing the conventional plain and DWI images to determine the solid part of each tumor and then matching the APTWI pseudo colored map with the DWI image of the corresponding layer and drawing a region of interest (ROI) based on the lesion contour displayed by the DWI image. The ROI was placed to cover as much of the solid part of the tumor as possible and to avoid large vessels and hemorrhagic, calcified, cystic and necrotic areas. The average MTRasym (3.5 ppm) of each tumor is the average of the measured values of each layer.

The APTWI signal can be calculated by the following equation [26]:

$$\text{MTRasym (3.5 ppm)} = [S_{sat}(-3.5_{ppm}) - S_{sat}(+3.5_{ppm})]/S_0,$$

where MTRasym is the asymmetric magnetization transfer ratio, $S_{sat}$ is the signal strength after the saturation pulse is applied, and $S_0$ is the signal strength without the saturation pulse applied [13,16].

### 2.4. Statistical analysis

All statistical analyses were performed using SPSS 23.0 (SPSS, Chicago, IL, USA) and MedCalc version 11.1.1.0 for Windows (MedCalc software, Mariakerke, Belgium). A Bland-Altman plot was used to evaluate the consistency of the results measured by the 2 physicians. The Kolmogorov-Smirnov test was used to evaluate the normality of the distribution of the measurement data, and normally distributed data are expressed as $\bar{X} \pm S$. The independent-sample *t*-test was used to determine differences in the MTRasym (3.5 ppm) between CSC and CA. ANOVA was used to compare the MTRasym (3.5 ppm) among G1, G2, and G3 CSC, followed by Dunnett's *t*-test for between-group comparisons. ROC curve analysis was used to evaluate the diagnostic performance of the MTRasym (3.5 ppm). Spearman correlation analysis was used to analyze the correlation between the MTRasym (3.5 ppm) and the grade of CSC differentiation. $P < 0.05$ was considered statistically significant.

## 3. Results

### 3.1. Patient and lesion characteristics

The histological diagnoses of the tumors excised from the 76 patients included in this study demonstrated that 60 patients had CSC (20 had G3 CSC, 23 had G2 CSC, and 17 had G1 CSC), and 16 patients had CA (13 had G3 CA, and 3 had G2 CA). Among the tumors, in 12 cases of G3 CSC, 3 cases of G2 CSC and 2 cases of G1 CA, obvious areas of cystic necrosis were observed; in 9 cases of G3 CSC, 2 cases G2 CSC and 3 cases G3 CA, a small area of bleeding was observed.

The tumor volume in the 60 CSC patients was 41.6 ± 29.6 $cm^3$; the high-level and low-level tumor volumes were 39.8 ± 29.1 $cm^3$ and 43.2 ± 26.8 $cm^3$, respectively. The tumor volume in the 16 patients with CA was 37.3 ± 31.4 $cm^3$. No significant differences in tumor volume were observed among the groups.

### 3.2. Interobserver agreement

The MTRasym (3.5 ppm) and tumor volume measured by the two readers showed good consistency, with 14/16 (87.5%, CA), 17/20 (85.0%, high-level CSC), 35/40 (87.5%, low-level CSC), 15/16 (93.8%, CA), 18/20 (90.0%, high-level CSC), and 35/40 (87.5%, low-level CSC) cases within the limit of 95% consistency (Fig. 2); therefore, the averages of the MTRasym (3.5 ppm) and tumor volume measured by the two readers were taken as the final data.

### 3.3. Parameter comparison

No significant differences in age were found among the groups (Tables 1, 2 and 3). The MTRasym (3.5 ppm) was higher in CA than that in CSC ($P = 0.001$). The MTRasym (3.5 ppm) was higher in high-level CSC than that in low-level CSC ($P = 0.001$). The MTRasym (3.5 ppm) was positively correlated with the grade of CSC differentiation ($r = 0.498$, $P = 0.001$, Fig. 3). The MTRasym (3.5 ppm) was higher in G3 CSC than that in G1 and G2 CSC ($P = 0.02/0.01$). No significant difference in the MTRasym (3.5 ppm) was found between G2 CSC and G1 CSC ($P = 0.173$) (Tables 1, 2 and 3, Fig. 4).

### 3.4. ROC analysis

The AUC for the MTRasym (3.5 ppm) for distinguishing CSC and CA was 0.779, with a cut-off, sensitivity, and specificity of 2.97%, 60.0% and 82.5%, respectively, and a 95% confidence interval of 0.609–0.904. The AUC for the MTRasym (3.5 ppm) for distinguishing high-/low-level CSC was 0.756, with a cut-off, sensitivity, and specificity of 3.29%, 68.8% and 83.3%, respectively, and a 95% confidence interval of 0.648–0.909 (Fig. 5, Table 4).

## 4. Discussion

### 4.1. Comparison of CA and CSC

In this research, we found that the MTRasym (3.5 ppm) in CA was generally higher than that in CSC, which is consistent with a previous study using CEST to identify squamous carcinoma and adenocarcinoma in the lungs reported by Ohno et al. [27]. In principle, only mobile proteins and peptides (such as those in the cytoplasm) can result in characteristic amide proton resonance [12]. These findings indicate that compared with CSC tissue, CA tissue has a higher mobile protein/peptide content or a faster exchange rate between its amide protons and free water protons.

APT-weighted hyperintensity in gliomas [17–20] and other cancers [21–23] was previously assumed to be associated with high tumor cellularity.

Additionally, Togao et al. [28,34] found that tissue necrosis will

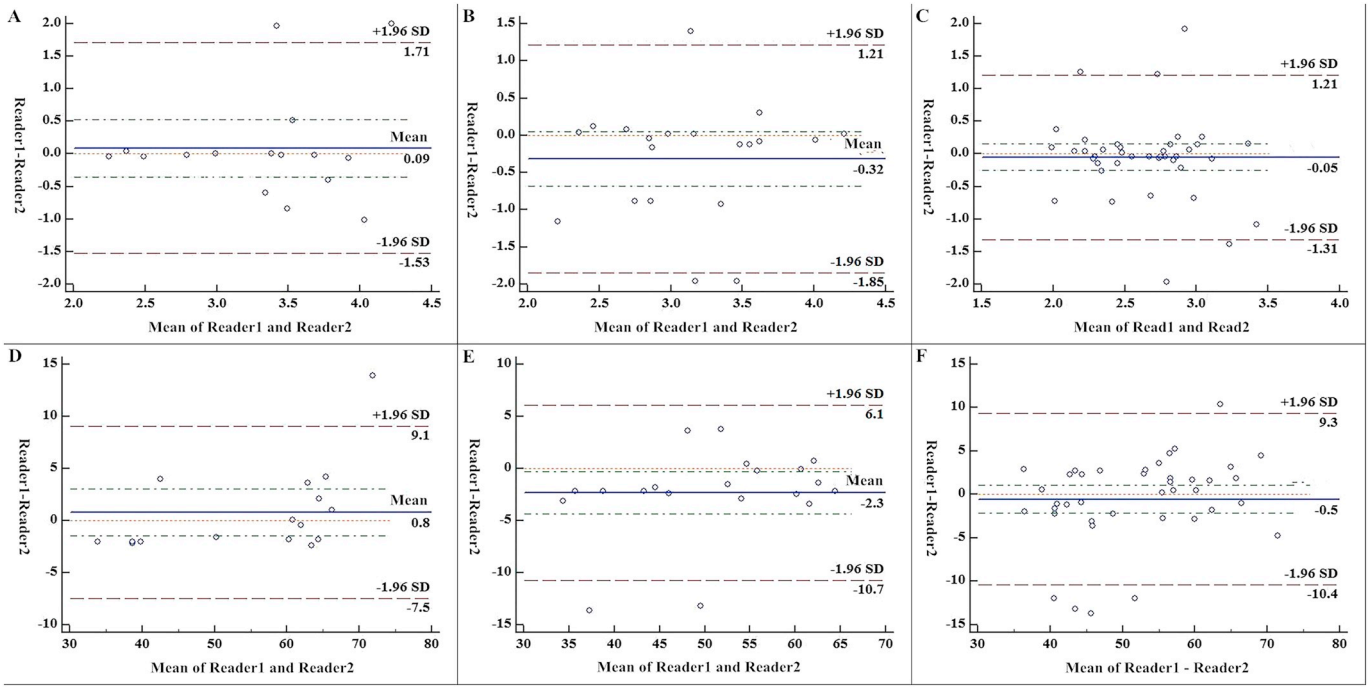


**Fig. 2.** Bland-Altman diagram of MTRasym (3.5 ppm) and tumor volumes measured by 2 Observers: A/B/C represent the consistency analysis of the MTRasym (3.5 ppm) measured by two observers. A represents the CA group, B represents the high-level CSC group, and C represents the low-level CSC group. D/E/F represent the consistency analysis of the tumor volumes measured by two observers. A represents the CA group, B represents the high-level CSC group, and C represents the low-level CSC group.

**Table 1**
Comparison of MTRasym values of CSC and CA.

| Group | Case | Age | MTRasym (%) |
|---|---|---|---|
| CA group | 16 | 58.62 ± 7.73 | 3.32 ± 0.59 |
| CSC group | 60 | 60.53 ± 8.99 | 2.80 ± 0.49 |
| *t* value | | 0.775 | −3.599 |
| P value | | 0.441 | 0.001 |

CSC: cervical squamous carcinoma, CA: cervical adenocarcinoma.

**Table 2**
Comparison of MTRasym values in high/low CSC groups.

| Group | Case | Age | MTRasym (%) |
|---|---|---|---|
| High CSC group | 20 | 61.45 ± 8.93 | 3.14 ± 0.53 |
| Low CSC group | 40 | 60.08 ± 9.10 | 2.63 ± 0.37 |
| *t* value | | −0.555 | −4.300 |
| P value | | 0.581 | 0.001 |

CSC: cervical squamous carcinoma, CA: cervical adenocarcinoma.

**Table 3**
Comparison of MTRasym values in well-/moderately/poorly differentiated CSC groups.

| Group | Case | Age | MTRasym (%) |
|---|---|---|---|
| Well-differentiated CSC group | 17 | 62.88 ± 10.23 | 2.51 ± 0.30 |
| Moderately differentiated CSC group | 23 | 58.00 ± 7.76 | 2.72 ± 0.39 |
| Poorly differentiated CSC group | 20 | 61.45 ± 8.93 | 3.14 ± 0.53 |
| *F* value | | 1.630 | 10.696 |
| P value | | 0.205 | 0.001 |

CSC: cervical squamous carcinoma, CA: cervical adenocarcinoma. Note: P = 0.173 between the well- and moderately differentiated CSC groups, P = 0.02 between the moderately and poorly differentiated CSC groups, and P = 0.01 between the well- and poorly differentiated CSC groups.

lead to the release of more mobile proteins and peptides into the surrounding environment. However, the above information cannot fully explain the results of this experiment because compared with CSC, CA is less dense and less prone to necrosis. Therefore, we can speculate that the reason for the increase in the MTRasym (3.5 ppm) for CA is that such tumors have strong protein secretion ability, which is consistent with the physiological characteristics of cervical gland cells, which have a rich glandular structure and secrete a large amount of mucin [29].

At present, no studies have discussed whether differences in the protein/peptide secretion ability of tumor cells cause changes in the MTRasym (3.5 ppm). We speculate that this gap may exist because relevant studies have mostly targeted tumors of the same type with different grades, and the protein/peptide secretion ability of tumor cells does not substantially vary. Compared to such studies, in the present research, APT was applied to study different types of UCC, and the results show that the difference in the ability of cells to secrete proteins/peptides may have considerable significance in the identification of different types of tumors. The pH is another important factor affecting the MTRasym (3.5 ppm). If the pH varies within a certain range, higher levels are more favorable for proton exchange than lower levels [17–19]. However, no authoritative study has proven that a difference in pH exists between CA and CSC tissues. Nevertheless, some studies have shown that CA has a loose cell structure and a high microvascular density (MVD) and is less prone to ischemic necrosis, while CSC has a high cell density, faster proliferation rate, and a lower MVD and is prone to ischemic necrosis [29]. In this study, the proportion of CSC lesions with liquefactive necrosis (15/60) was greater than that of CA lesions (3/16), which supports this view. Therefore, we can speculate that CSC easily leads to oxygen-deficient conditions in tissue, which may induce a local acidic environment, thus affecting the exchange rate of amino protons.

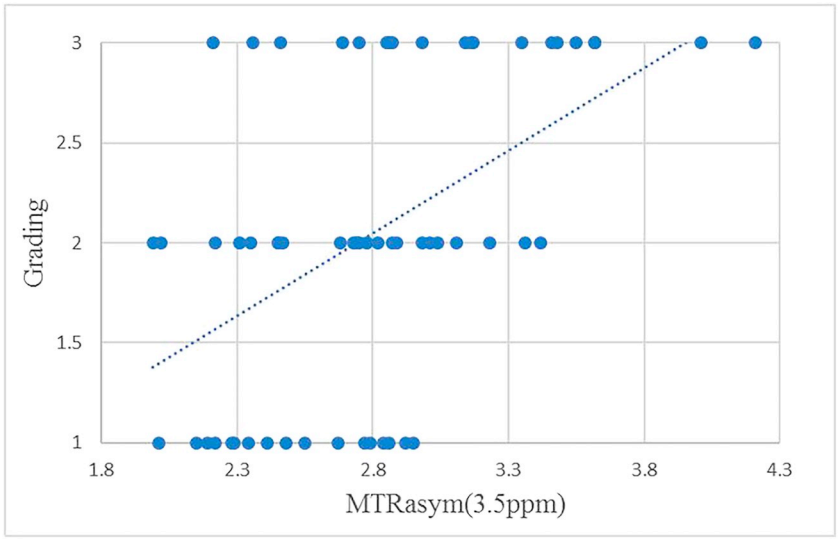


**Fig. 3.** Correlation between MTRasym (3.5 ppm) and grade of CSC differentiation (r = 0.498, P = 0.001).

### *4.2. Comparison of different grades of CSC differentiation*

The results of this research also show that the MTRasym (3.5 ppm) has a relatively weak positive relation with the tumor differentiation grade (r = 0.498, P = 0.001); the MTRasym (3.5 ppm) in low-level CSC was lower than that in high-level CSC (P = 0.001). However, no significant difference in the MTRasym (3.5 ppm) was identified between G2 CSC and G1 CSC (P = 0.173). This finding is similar to that of

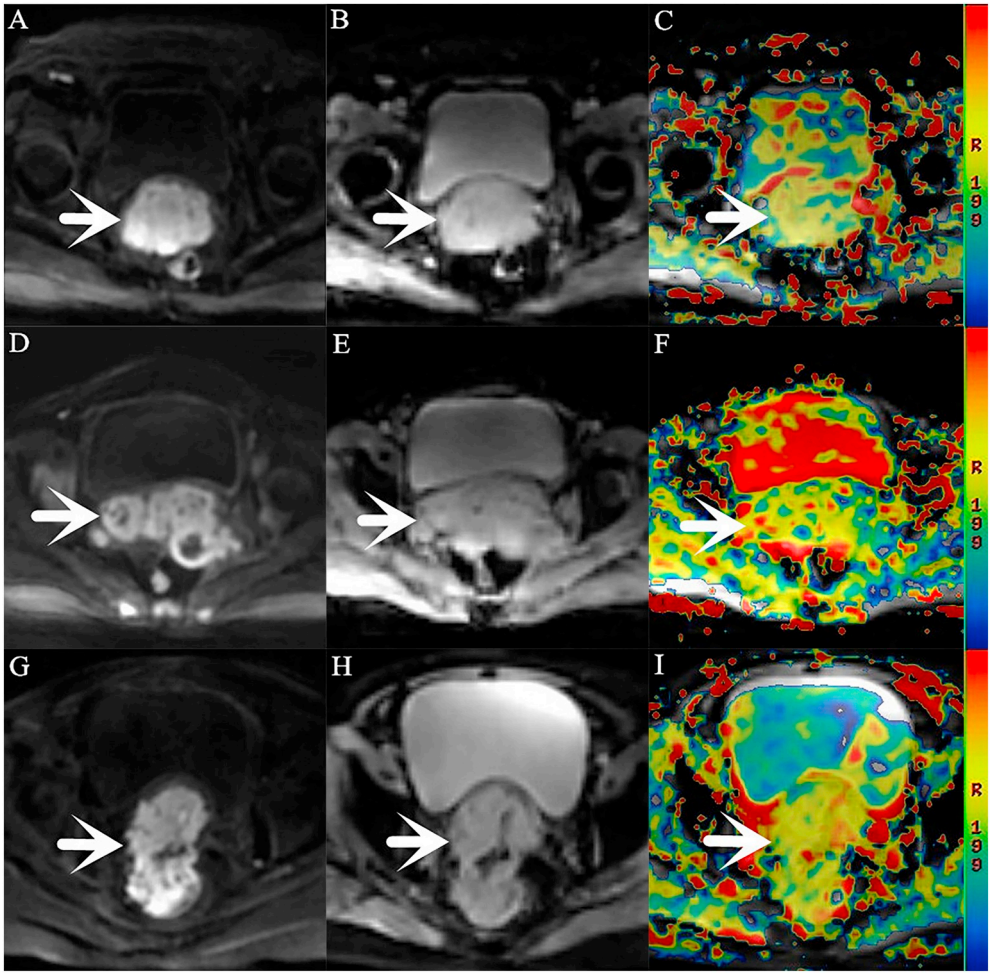


**Fig. 4.** A/D/G are DWI images (b = 1000 s/mm$^2$), B/E/H are original APT images, C/F/I are APT pseudo colored maps; (A–C) Female, 52 years old, well-differentiated CSC (arrow head), MTRasym = 2.77%; (D–F) female, 58 years old, moderately differentiated CSC (arrow head), MTRasym = 3.55%; (G–I) female, 64 years old, poorly differentiated CA (arrow head), MTRasym = 3.88%.

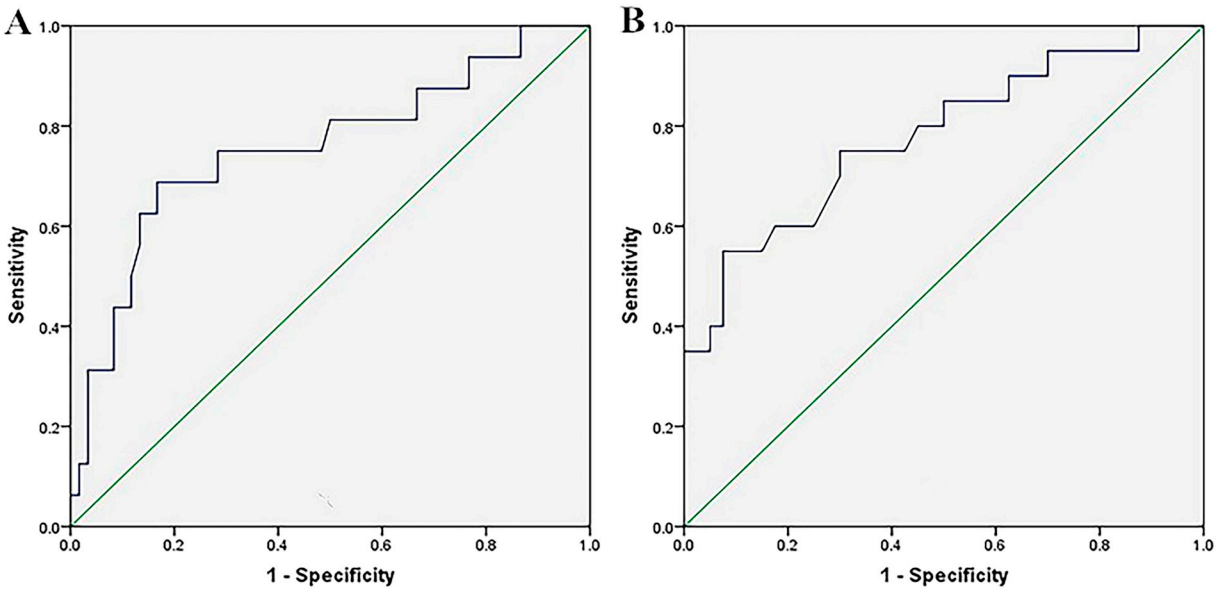


**Fig. 5.** (a) ROC curve of the MTRasym (3.5 ppm) in identifying CSC and CA; (b) ROC curve of the MTRasym (3.5 ppm) in identifying high and low CSC.

**Table 4**
Diagnostic performance of MTRasym value.

| Parameters | AUC | Threshold (P value) | Sensitivity (%) | Specificity (%) | 95% confidence interval |
|---|---|---|---|---|---|
| Identifying CSC/CA | 0.756 | 3.29 (0.002) | 68.8 | 83.3 | 0.609–0.904 |
| Identifying high/low CSC | 0.779 | 2.97 (0.000) | 60.0 | 82.5 | 0.648–0.909 |

CSC: cervical squamous carcinoma, CA: cervical adenocarcinoma.

Takayama et al. [30] in predicting the grade of endometrial cancer with APTWI and that of Zou et al. [31] in predicting the grade of glioma with APTWI, indicating that APTWI can be used to preliminarily evaluate the pathological differentiation of CSC. The grade of CSC differentiation is correlated with cell density and nuclear atypia. Cell density has been proven to be one of the important factors affecting the MTRasym (3.5 ppm) of tumor tissues by a large number of studies [17–20]; greater tumor tissue malignancy corresponds to greater cell density, greater protein/polypeptide secretion, and a higher MTRasym (3.5 ppm). Meanwhile, nuclear atypia has been reported to cause interactions between hydrophobic cell membranes and macromolecular substances [32,33], promoting the release of proteins and polypeptides. In addition, a lower tumor differentiation grade corresponds to a greater probability of tissue necrosis. In this study, the incidence of liquefactive necrosis was greater in high-level CSC (12/20) than that in low-level CSC (3/40), which supports this view. Togao et al. [28,34] applied APTWI to examine glioma and showed that the MTRasym (3.5 ppm) of tumor tissues with necrosis identified by microscopy was higher than that of tissues without or with less necrosis, which may be correlated with the proteins and polypeptides released during tissue necrosis. However, factors that are not conducive to an increase in the MTRasym (3.5 ppm) remain in poorly differentiated tumors. Suzuki et al. [35] considered that an acidic pH can increase the invasiveness of tumor cells and that poorly differentiated tumors and highly malignant tumors may have lower pH levels. At the same time, with a decreased degree of differentiation, tumor tissue is more prone to oxygen deficiency, which may lead to the formation of a local acidic environment, further reducing the pH. Lower pH levels are not conducive to proton exchange. In summary, the difference in the MTRasym (3.5 ppm) among UCC tumors with different degrees of differentiation is caused by a variety of factors. Among the various factors that can lead to an increase in the MTRasym (3.5 ppm), cell density predominates, while factors leading to a decrease in the MTRasym (3.5 ppm), such as low pH levels, have less influence. Thus, the MTRasym (3.5 ppm) increases gradually as the CSC differentiation grade decreases.

### 4.3. Limitations

This research has the following limitations: (1) Single APTWI scans can only provide single-layer images; to fully visualize a tumor, multiple scans must be performed, which increases the scanning time. (2) The APTWI sequence used in this research is derived from the EPI sequence, which has poor resolution and a low signal-to-noise ratio and is vulnerable to motion/air/metal image artifacts, leading to poor detection of very small lesions. To some extent, these factors affect the accuracy of the experiment. In the future, we will consider rapid imaging methods to shorten the scanning time and reduce motion artifacts, as well as saturation band techniques to reduce air artifacts. (3) Due to the small number of cases, only a comparative analysis of CSC and CA was conducted in this research, and no other rare cervical tumors, such as adenosquamous carcinoma, were included. At the same time, no detailed classification was applied for the different types of CSC and CA. In the future, more pathological examinations will be included for more detailed research.

## 5. Conclusion

In conclusion, with the development of MRI, a series of advanced technologies, such as MRI texture feature analysis [36] and intravoxel incoherent motion (IVIM) [24], among others, have been used to assess the stage, grade, and pathological type of UCC in recent years. Compared with the above modalities, APTWI has unique advantages for displaying the metabolism of diseased proteins and has the potential to be used as a supplementary method for evaluating and guiding clinical treatment for UCC lesions.

## Abbreviations

| | |
|---|---|
| UCC | uterus cervical cancer |
| CSC | cervical squamous carcinoma |
| CA | cervical adenocarcinoma |
| APTWI | amide proton transfer-weighted imaging |
| MRI | magnetic resonance imaging |
| MRS | magnetic resonance spectroscopy |
| CEST | chemical exchange saturation transfer |
| AUC | area under the curve |
| ROC | receiver operating characteristic |
| ROI | region of interest |
| MTRasym | magnetization transfer ratio |

## Acknowledgements

We acknowledge the support received from the Henan Medical Science and Technology Research Program. In addition, Nan Meng is especially grateful for the patience, care, and support received from Jing Sun over the past few years. Will you marry me?

## Funding

This work was supported by the Henan Medical Science and Technology Research Program [grant numbers 2018020357 and 2018020367].

## Competing interests

The authors declare that they have no competing interests.

## References

[1] Fitzmaurice C, Dicker D, Pain A, Hamavid H, Moradi-Lakeh M, MacIntyre MF, et al. The global burden of cancer 2013. JAMA Oncol 2015;1:505–27.
[2] Maruthappu M, Head MG, Zhou CD, Gilbert BJ, El-Harasis MA, Raine R, et al. Investments in cancer research awarded to UK institutions and the global burden of cancer 2000–2013: a systematic analysis. BMJ Open 2017;7:e013936.
[3] Hu SY, Zheng RS, Zhao FH, Zhang SW, Chen WQ, Qiao YL. Trend analysis of cervical cancer incidence and mortality rates in Chinese women during 1989–2008. Zhongguo Yi Xue Ke Xue Yuan Xue Bao 2014;36:119–25.
[4] Noh JM, Park W, Kim YS, Kim JY, Kim HJ, Kim J, et al. Comparison of clinical outcomes of adenocarcinoma and adenosquamous carcinoma in uterine cervical cancer patients receiving surgical resection followed by radiotherapy: a multicenter retrospective study (KROG 13-10). Gynecol Oncol 2014;132:618–23.
[5] Sindos M, Pisal N, Freeman-Wang T, Singer A. Cervical cancer: effect of glandular cell type on prognosis, treatment, and survival. Obstet Gynecol 2003;101. [1354-5 author reply 1355].
[6] Gruen A, Musik T, Köhler C, Füller J, Wendt T, Stromberger C, et al. Adjuvant chemoradiation after laparoscopically assisted vaginal radical hysterectomy (LARVH) in patients with cervical cancer: oncologic outcome and morbidity. Strahlenther Onkol 2011;187:344–9.
[7] Zhang N, Gao Y, Yan X, Institute. Evaluation of the effectiveness and safety of postoperative chemotherapy for stage I B1-IIA cervical cancer. J Pract Obstet Gynecol 2014;30(1):21–5.
[8] Kalliala I, Anttila A, Nieminen P, Halttunen M, Dyba T. Pregnancy incidence and outcome before and after cervical intraepithelial neoplasia: a retrospective cohort study. Cancer Med 2014;3:1512–6.
[9] Moukarzel LA, Angarita AM, VandenBussche C, Rositch A, Thompson CB, Fader AN, et al. Preinvasive and invasive cervical adenocarcinoma: preceding low-risk or negative pap result increases time to diagnosis. J Low Genit Tract Dis 2017;21:91–6.
[10] Pappa KI, Christou P, Xholi A, Mermelekas G, Kontostathi G, Lygirou V, et al. Membrane proteomics of cervical cancer cell lines reveal insights on the process of cervical carcinogenesis. Int J Oncol 2018;53:2111–22.
[11] Andronesi OC, Arrillaga-Romany IC, Ly KI, Bogner W, Ratai EM, Reitz K, et al. Pharmacodynamics of mutant-IDH1 inhibitors in glioma patients probed by in vivo 3D MRS imaging of 2-hydroxyglutarate. Nat Commun 2018;9:1474.
[12] Yan K, Fu Z, Yang C, et al. Assessing amide proton transfer (APT) MRI contrast origins in 9 L gliosarcoma in the rat brain using proteomic analysis[J]. Mol Imaging Biol 2015;17(4):479.
[13] Zhou J, Zhu H, Lim M, et al. Three-dimensional amide proton transfer MR imaging of gliomas: initial experience and comparison with gadolinium enhancement[J]. J Magn Reson Imaging 2013;38(5):1119–28.
[14] Zhou J, Payen JF, Wilson DA, Traystman RJ, van Zijl PC. Using the amide proton signals of intracellular proteins and peptides to detect pH effects in MRI. Nat Med 2003;9:1085–90.
[15] Jiang S, Yu H, Wang X, Lu S, Li Y, Feng L, et al. Molecular MRI differentiation between primary central nervous system lymphomas and high-grade gliomas using endogenous protein-based amide proton transfer MR imaging at 3 Tesla. Eur Radiol 2016;26:64–71.
[16] Zhou J, Heo HY, Knutsson L, et al. APT-weighted MRI: techniques, current neuro applications, and challenging issues[J]. J Magn Reson Imaging 2019. https://doi.org/10.1002/jmri.26645.
[17] Su C, Zhao L, Li S, Jiang J, Cai K, Shi J, et al. Amid proton transfer (APT) and magnetization transfer (MT) MRI contrasts provide complimentary assessment of brain tumors similarly to proton magnetic resonance spectroscopy imaging (MRSI). Eur Radiol 2019;29(3):1203–10.
[18] Jiang S, Eberhart CG, Zhang Y, et al. Amide proton transfer-weighted magnetic resonance image-guided stereotactic biopsy in patients with newly diagnosed gliomas.[J]. Eur J Cancer 2017;83:9–18.
[19] Sakata A, Okada T, Yamamoto A, Kanagaki M, Fushimi Y, Okada T, et al. Grading glial tumors with amide proton transfer MR imaging: different analytical approaches. J Neurooncol 2015;122:339–48.
[20] Jiang S, Eberhart CG, Lim M, et al. Identifying recurrent malignant glioma after treatment using amide proton transfer-weighted MR imaging: a validation study with image-guided stereotactic biopsy[J]. Clin Cancer Res 2019;25(2):552–61.
[21] Law B, King AD, Ai QY, Poon D, Chen W, Bhatia KS, et al. Head and neck tumors: amide proton transfer MRI. Radiology 2018;288:782–90.
[22] Takayama Y, Nishie A, Sugimoto M, Togao O, Asayama Y, Ishigami K, et al. Amide proton transfer (APT) magnetic resonance imaging of prostate cancer: comparison with Gleason scores. MAGMA 2016;29:671–9.
[23] Nishie A, Takayama Y, Asayama Y, Ishigami K, Ushijima Y, Okamoto D, et al. Amide proton transfer imaging can predict tumor grade in rectal cancer. Magn Reson Imaging 2018;51:96–103.
[24] Dappa E, Elger T, Hasenburg A, et al. The value of advanced MRI techniques in the assessment of cervical cancer: a review. Insights Imaging 2017;8(5):471–81.
[25] Togao O, Hiwatashi A, Keupp J, Yamashita K, Kikuchi K, Yoshiura T, et al. Scan-rescan reproducibility of parallel transmission based amide proton transfer imaging of brain tumors. J Magn Reson Imaging 2015;42:1346–53.
[26] Tee YK, Donahue MJ, Harston GW, Payne SJ, Chappell MA. Quantification of amide proton transfer effect pre- and post-gadolinium contrast agent administration. J Magn Reson Imaging 2014;40:832–8.
[27] Ohno Y, Yui M, Koyama H, Yoshikawa T, Seki S, Ueno Y, et al. Chemical exchange saturation transfer MR imaging: preliminary results for differentiation of malignant and benign thoracic lesions. Radiology 2016;279:578–89.
[28] Togao O, Yoshiura T, Keupp J, Hiwatashi A, Yamashita K, Kikuchi K, et al. Amide proton transfer imaging of adult diffuse gliomas: correlation with histopathological grades. Neuro Oncol 2014;16:441–8.
[29] Argüello-Ramírez J, Pérez-Cárdenas E, Delgado-Chávez R, Solorza-Luna G, Villa-Treviño S, Arenas-Huertero F. Matrix metalloproteinases-2, -3, and -9 secreted by explants of benign and malignant lesions of the uterine cervix. Int J Gynecol Cancer 2004;14:333–40.
[30] Takayama Y, Nishie A, Togao O, Asayama Y, Ishigami K, Ushijima Y, et al. Amide proton transfer MR imaging of endometrioid endometrial adenocarcinoma: association with histologic grade. Radiology 2018;286:909–17.
[31] Zou T, Yu H, Jiang C, Wang X, Jiang S, Rui Q, et al. Differentiating the histologic grades of gliomas preoperatively using amide proton transfer-weighted (APTW) and intravoxel incoherent motion MRI. NMR Biomed 2018;31.
[32] Tang Y, Dundamadappa SK, Thangasamy S, Flood T, Moser R, Smith T, et al. Correlation of apparent diffusion coefficient with Ki-67 proliferation index in grading meningioma. AJR Am J Roentgenol 2014;202:1303–8.
[33] Whittaker CS, Coady A, Culver L, Rustin G, Padwick M, Padhani AR. Diffusion-weighted MR imaging of female pelvic tumors: a pictorial review. Radiographics 2009;29:759–74. [discussion 774-8].
[34] Togao O, Hiwatashi A, Yamashita K, Kikuchi K, Keupp J, Yoshimoto K, et al. Grading diffuse gliomas without intense contrast enhancement by amide proton transfer MR imaging: comparisons with diffusion- and perfusion-weighted imaging. Eur Radiol 2017;27:578–88.
[35] Suzuki A, Maeda T, Baba Y, Shimamura K, Kato Y. Acidic extracellular pH promotes epithelial mesenchymal transition in Lewis lung carcinoma model. Cancer Cell Int 2014;14:129.
[36] Zhou Y, Liu J, Liu C, Jia J, Li N, Xie L, et al. Intravoxel incoherent motion diffusion weighted MRI of cervical cancer correlated with tumor differentiation and perfusion. Magn Reson Imaging 2016;34(8):1050–6.